ROAD ENGINEERING ASSOCIATION OF ASIA & AUSTRALASIA

JOURNAL

ISSN : 1394 -1054

PP 7021/8/94

No. 6

ROAD ENGINEERING ASSOCIATION OF ASIA & AUSTRALASIA

Journal

July 1995

Governing Council 1995/1998

President
- Dr. Robin Dunlop

Vice-Presidents
- Tan Sri Dato' Wan A. Rahman Yaacob
- Mr. Rod Payze

Immediate Past-President
- Mr. Arthur Y. Chen

Past-President
- Dr. Tan Swan Beng

Honorary Secretary-General
- Mr. Wong Wai Ching

Honorary Treasurer-General
- Dr. Za-Chieh Moh

Members
- Japan Road Association
- China Road Federation
- Indonesian Road Development Association
- Korea Highway Corporation
- Public Works Department Singapore
- Public Works Department Brunei Darussalam
- Roads Association of Thailand
- Road Engineering Association of Philippines
- Ret-Ser Engineering Agency
- Express Highway Research Foundation of Japan
- Chairman, REAAA Australian Chapter
- Dr. Ian Johnston
- Mr. Mah Guan Seng
- Mr. Chen Choong Lee

JOURNAL

Publisher
- THE ROAD ENGINEERING ASSOCIATION OF ASIA & AUSTRALASIA
  Unit A2-22, Block A, 2nd floor
  P.J. Industrial Park, Jalan Kemajuan
  Section 13, 46200 Petaling Jaya
  Selangor, Malaysia

  Tel: 60-3-7571159
  Fax: 60-3-7575011

Printer
- Percetakan Bahagia
  3 Jalan Jejaka Dua, Taman Maluri
  Kuala Lumpur

Lay-Out
- AC Designers Sdn. Bhd.

COVER: Spiral ramps on Metropolitan Expressway, Japan.

The Katahira Awards

The late Mr. Nobutaka Katahira, a past President of REAAA generously willed ¥ 3.0 million to REAAA, which is now kept in fixed deposit known as the Katahira Fund.

The REAAA Governing Council has decided that the interest accruing from the above Fund be used to finance the Katahira Awards, which will be presented to the three best technical papers from young authors presented during each REAAA Conference.

The Katahira Awards were given for the first time during the 7th REAAA Conference held in June 1992 in Singapore. Three technical papers which won the awards at the 8th REAAA Conference held in April 1995 in Taipei are:-

1. "An Assessment of The Effect of Contraflow Bus Lane on Ridership" by Shyue Koong Chang and Hsin-Hsiung Chen.

2. Electronic Toll Collection in Hong Kong" by W.K. Lam

3. Simultaneous Measurement of Thermal Conductivity and Thermal Diffusivity of Pavement Materials" by Low Boon-Hwee, Fwa Tien-Fang and Tan Siew-Ann.

The three papers above are reprinted in this issue of the Journal to benefit those members who were not at the Conference.

An Assessment of The Effect of Contraflow Bus Lane on Ridership

by
Shyue Koong Chang
Associate Professor
Department of Civil Engineering
National Taiwan University, Taiwan, R.O.C.

and
Hsin Hsiung Chen
Ph. D. Candidate
Department of Civil Engineering
National Taiwan University, Taiwan, R.O.C.

Abstract

Contraflow bus lanes have been implemented in Taipei City since February 1990. Effects of this bus priority strategy have been analyzed in related works. This paper presents new evidence of the impacts of the contraflow bus lanes on bus ridership. Time-series model has been developed for this evaluation. The study focuses on one bus line with very minor changes before and after the implementation of contraflow bus lane. General information of the bus priority strategy is provided. Monthly ridership data were collected. Box-Jenkins modelling techniques are used to forecast the ridership that would have resulted if the contraflow lane was not implemented. Effects of the contraflow bus lane on ridership are identified based on comparison between the forecasted ridership and actual ridership. It is shown that ridership of the bus line assessed had significantly increased about 28.5 percent after implementation of the bus lane. The trend of this significant effect has also been explored.

Introduction

Taipei is facing serious traffic congestion problems. In addition to a mass rapid transit system, various transportation system management (TSM) alternatives have continuously been implemented. Among the TSM actions, implementation of two contraflow bus lanes on arterial streets was most notable. Taipei Transportation Department and public transit authorities in other cities are interested in understanding the related benefits for bus users and bus operators, since more than 50 percent of work trips, i.e. 2.2 millions of trips per day, use buses as their commuting mode in the Taipei metropolitan area.

The two contraflow bus lanes have been implemented on two major arterial streets since February 1990. These two arterials, namely Xin-Yi Road and Zen-Eye Road, are parallel and connect the old CBD in the western area and the new developing area in the eastern district of Taipei. The contraflow bus lanes are implemented progressively so as to integrate with comprehensive design of one-way street network. Currently, the contraflow bus lane is exclusively designed for buses, not for other high-occupancy vehicles.

General features of the bus lanes have been presented in related works (1, 2, 3). A brief review is presented here for convenience. Figure 1 shows the existing layout of Xin-Yi Road in which one contraflow bus lane (with width of 3.5m), three "pure" car lanes (3.25m), and two mixed-traffic lanes (5m) are included. It should be noted that the Xin-Yi Road was a two-way six-lane arterial before it was modified to be a one-way street. It can be observed that the mixed-traffic lanes and "pure" car lanes are separated by a wide area because of heavy proportion of motorcycles.

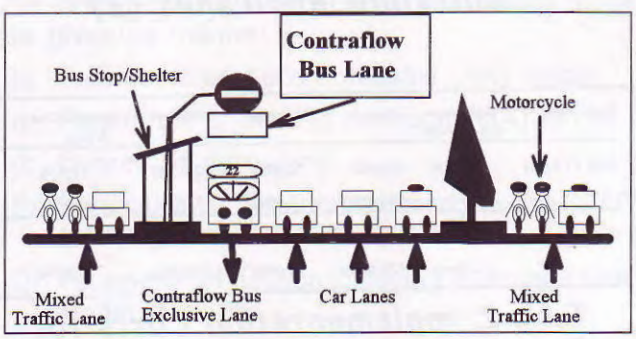

*Figure 1: **Contraflow Bus Lane on Xin-Yi Road, Taipei***

Zen-Eye Road has a similar geometric layout for the bus lane in most of its sections. Currently, all buses driving on the bus lane in their inbound (outbound) direction have to drive on the mixed-traffic lane for their outbound (inbound) direction.

Table 1 shows that Xin-Yi Road has a longer exclusive bus lane, more bus routes, more bus stops, more bus ridership, and more vehicle volumes than for Zen-Eye Road. It should be noted that the bus volumes and ridership are varying over different street segments. It can also be shown that average stop spacings are 0.40 km and 0.64 km for Xin-Yi and Zen-Eye, respectively.

Costs of developing the two bus lanes are also compared, as shown in Table 2. It is shown that the average costs per km are 18,750 and 12,630 dollars for Xin-Yi and Zen-Eye, respectively. A major component of the total implementation cost is the bus stops and shelters. It covers more than 80 percent of the total implementation cost for both arterials. It can also been shown that the average cost for each stop is about 66,000 dollars.

Effects of this bus priority strategy on ridership have been analyzed in a related work (3). This paper presents new evidence of the impacts of the contraflow bus lane. Ridership data for one bus line are collected for this analysis. In the following sections, problems of ignoring time variation in impact evaluation are identified. Ridership data and Box-Jenkins modelling techniques are presented. Analysis results are shown and discussed. Conclusions and suggested further studies are presented.

Road Name	Length (km)	No. of Bus Routs	No. of Stops	Bus Frequency at Peak Hour[1]	Ridership at Peak Hour[1]	Veh. Volumes at Peak Hour[2]
Xin-Yi Road	4.4	16	11	80 ~ 141	3,900 ~ 5,500	1,140
Zen-Eye Road	3.2	10	5	38 ~ 77	1,650 ~ 3,850	900

Note: 1. Varying with road sections. 2. in units of pcu per lane.

Table 1: General Information for Taipei Contraflow Bus Lanes (3)

Road Name	Bus Stops and Shelters	Signs	Markings	Total Cost	Average Cost ($/km)
Xin-Yi Road	726,000	40,000	58,800	824,800	18,750
	(4.4 km)	(88.1%)	(4.8%)	(7.1%)	(100%)
Zen-Eye Road	330,000	32,400	42,800	405,200	12,630
	(3.2 km)	(81.4%)	(8.0%)	(10.6%)	(100%)

Table 2: Implementation Costs for Taipei Contraflow Bus Lanes (3)

Problem for Time Dependent Data

Time variation must be considered in assessing the effects of event, which is observed based on time dependent data. Conventional evaluation methods simply compare differences between, before and after data and generate results that might not represent the real effect. For example, a monthly ridership before the implementation of contraflow bus lane is simply compared with the ridership in the same month after the implementation of a contraflow bus lane, and the results show a specific increase in ridership. However, this result might be inaccurate, since the bus ridership may be normally decreasing when national income increases. The effect of national income, which is normally time dependent, must be filtered in evaluation of the bus lane effects (3).

The problem of conventional intervention analysis has been discussed in a related work (4) and can be explained by a case shown in Figure 2. The points denoted t_1 and t_2 are the sampling time points before and after the event (e.g., the implementation of contraflow bus lane). Q_1 and Q_2 are the ridership at t_1 and t_2, respectively. The conventional evaluation method only compares the difference between Q_1 and Q_2. Then, the result shows that the ridership increases to the amount $\Delta q_1 + \Delta q_2$. However, the quantity Δq_1 is affected by many other time-dependent factors, such as population, income, congestion, etc. The real effect of contraflow bus lane should be Δq_2. It is obvious that the conventional method may overestimate this effect. In the contrary example, the result of conventional method may under-estimate this effect.

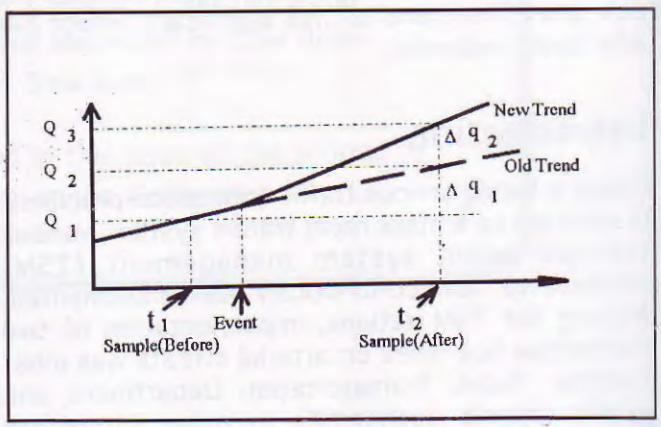

Figure 2: Effect of Event over Time (3)

Intervention Analysis

An evaluation approach based on time series method was used in this study. The trend of variation that would have resulted if the event had not occurred is estimated. This trend is then compared with the real trend of variation after the occurrence of event.

This evaluation method consists of four steps:

(1) Obtain the data before the occurrence of event. Assume the sample size of this data set was n. This time series data is noted as B_1, B_2, B_3,..., B_n.

(2) Assume that the event will not occur and forecast for the next m periods based on the collected data set B_1, B_2, B_3,..., B_n. The forecast data are noted as A_{n+1}, A_{n+2}, A_{n+3},..., A_{n+m}.

(3) Obtain the real time series data of the m periods after the event, that are labelled as C_{n+1}, C_{n+2}, C_{n+3},..., C_{n+m}.

(4) Conduct a comparison between these two time series: A_{n+1}, A_{n+2}, A_{n+3},..., A_{n+m}, and C_{n+1}, C_{n+2}, C_{n+3},..., C_{n+m}.

Data Analysis

A typical bus route (Route #22) is selected for this study since its route structure has very minor changes before and after the implementation of contraflow bus lanes. The monthly ridership data from January 1987 to October 1994 were collected (5). The first 37 data from January 1987 to January 1990 are considered as the before-event data, and the remaining 57 data from February 1990 to October 1994 are the after-event data, which are shown in Figure 3. It shows a pattern of seasonal variation on an annual basis. A decreasing trend in ridership before January 1990 and a rising trend after February 1990 can be observed. The implementation of the contraflow bus lane seems to have increased the ridership.

It can also be observed that the ridership in one month is much lower that in other months. This lower ridership appeared in February due to two reasons: (1) the winter break and Chinese new year, (2) the number of days in February is less than in other months. Therefore, the daily ridership is also obtained as shown in Figure 4. The variances have been smoothed and the effect of differences among months is clearer.

Forecasting

The time series analysis method is applied to forecast the ridership. Since the series of ridership are time dependent, the autocorrelation among data must be considered. The Box-Jenkins ARIMA time series model is very useful for such analysis. The ARIMA (Autoregressive Integrate Moving Average) model uses the Autocorrelation Function (ACF) and Partial Autocorrelation Function (PACF) to identify the parameters of model. The basic process of ARIMA model includes diagnosing, identification, estimation and forecasting. The mathematical description and applications of ARIMA model may be found in related works (6, 7, 8). The general model can be described as ARIMA(p,d,q)(P,D,Q)^s.

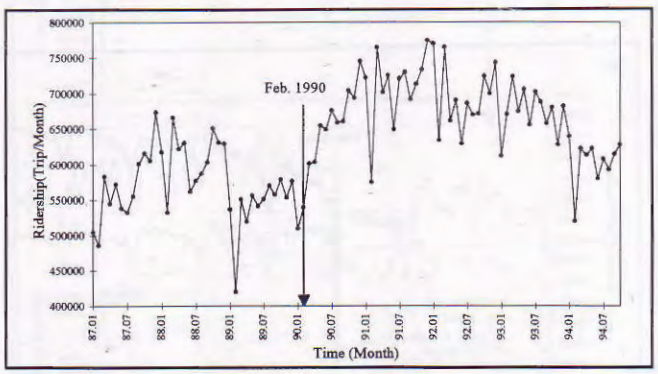

*Figure 3: **The Monthly Ridership Trend***

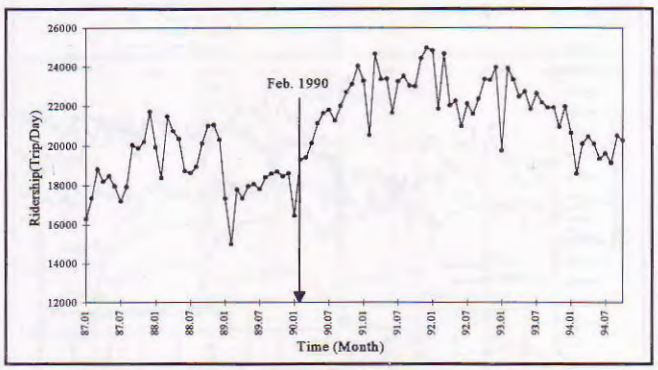

*Figure 4: **The Daily Ridership Trend***

The definitions of parameters in the ARIMA model are given as follows:

p: Parameter of Autoregressive (AR) Model

q: Parameter of Moving Average (MA) Model

d: Degree of difference

P: Parameter of Seasonal Autoregressive (SAR) Model (5)

Q: Parameter of Seasonal Moving Average (SMA) Model (6)

D: Degree of seasonal difference

s: Length of seasonal cycle

By using of the rule-of-thumb about ACF and PACF diagrams, the best model for the series of ridership per month can be obtained as ARIMA(1,0,0)(1,0,0)^{12}. The R^2 value of this model is 0.75, and all parameters in this model are statistically significant, given the 0.05 level of significance. Because the number of forcates is too large, we also relax the level as 0.15. This model is presented as follows:

$$Y_t = 0.87Y_{t-1} + 0.84Y_{t-12} + (0.87)(0.84)Y_{t-13} + 10451.5 \qquad (1)$$

(12.04) (13.35) (9.09) $R^2 = 0.75$

Based on this model, the ridership for the 57 months after implementation of the contraflow lane with both significance levels (i.e., from February 1990 to October 1994) were forecasted as shown in Fig. 5(a) and Fig. 5(b).

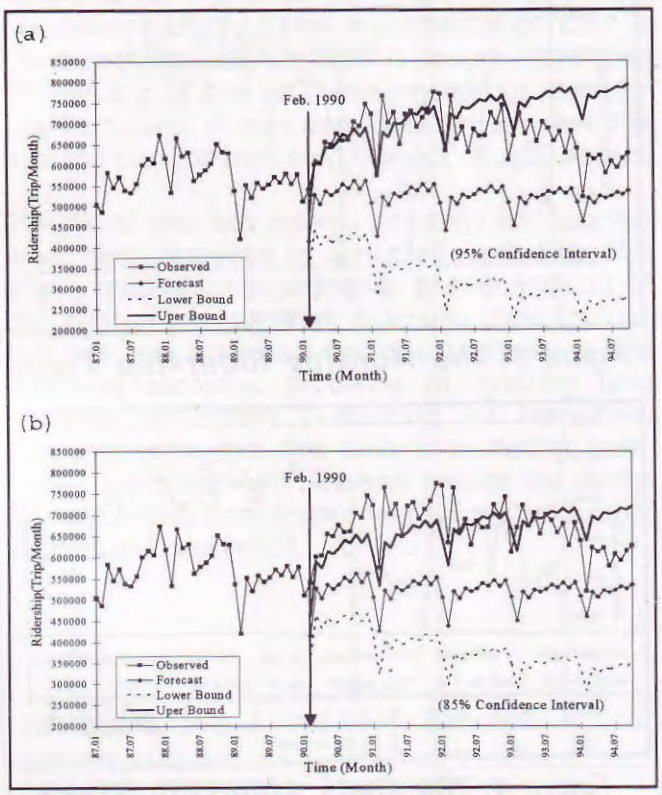

Figure 5: ***Forecast Results for Monthly Ridership***

The ARIMA model of daily ridership has also been obtained as ARIMA(1,0,0)(1,0,0)^{12}. The R^2 value of this model is 0.72, and all parameters are statistically significant. The model is given as

$$Y_t = 0.879Y_{t-1} + 0.769Y_{t-12} + (0.879)(0.769)Y_{t-13} + 467.86 \qquad (2)$$

(12.95) (8.64) (8.64) $R^2 = 0.72$

Based on this model, the forecast results are shown in Figure 6.

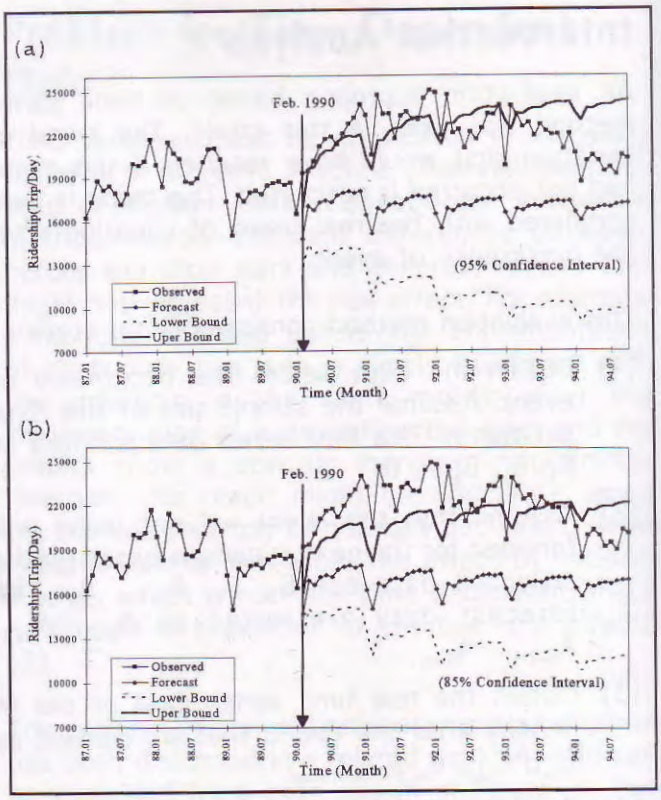

Figure 6: ***Forecast Results for Daily Ridership Evaluation***

The Box-Jenkins ARIMA model is developed and used to forecast the ridership that would have resulted if the contraflow lane was not implemented. The forecast ridership and actually observed ridership can then be compared, and the effects of the contraflow lane on ridership can be identified accordingly.

The comparison is conservatively conducted. The observed actual ridership is compared with the upper bounds of forecast ridership. The comparison results are given in Figure 7. In Fig. 7(a), all observed volumes are higher than forecast values, and 31 of them are even higher than the upper bounds of those forecast values. Comparison based on daily ridership is also shown in Fig. 7(c) and Fig. (7d). The results are similar to that of the monthly ridership. These results have already indicated a significant effect of the contraflow bus lane.

A statistical test for the differences between these two series data is also made. Because there is autocorrelation among the values of series data, the bias of test should be considered. But there is no statistical method to process a test about comparison of two time series data. The series of pairwise differences of the two series data is somewhat similar to a random process. Therefore it is assumed in the test that these differences

are random samples. Fisher Sign Test approach is then used for this nonparametric test. We only test the difference between of these two series data before March 1992 under 0.05 significance level, and before July 1993 under 0.15 significance level. The null hypothesis and alternative hypothesis of the first case are as follows:

H_0: There is no significant effect on ridership,

H_1: Not accept H_0.

It can be observed in Fig. 7(a) that there are 20 positive signs among these 26 differences of two series of data under 95 percent significance level. Therefore the cumulative probability can be obtain from the Binomial probability distribution as follows:

$$\sum_{i=0}^{6} B(26, i, 0.5) \cong 0.007$$

Therefore the null hypothesis H_0 is not accepted under the 0.05 level of significance, which implies that the bus ridership has significantly increased after implementation of the contraflow bus lane. The ridership increase is more significantly while using the forecasted series obtained under 0.15 level of significance.

The analysis results can also be used to indicate the weakness of conventional method for impact evaluation. The average ridership before and after the implementation of bus lane as well as the forecast ridership are given in Figure 8. When applying the conventional method, which is simply to compare the average ridership before and after the implementation of the bus lane, the effect will be underestimated, as shown in Table 3.

The comparison in Table 3 indicates that the effect of bus lane on ridership is 17.1 percent by the conventional method, while it is 28.5 percent based on the time series model developed in this study.

The trend of the effect has also been analyzed in order to identify whether the positive effect is increasing or decreasing. The growth rates for the average daily ridership after the implementation of bus lane are plotted in Figure 9. Within these two functions, the function in Fig. 9(b) is comparatively closed to the real trend. Although it is shown that the increase on ridership is getting steady after reaching a higher growth rate of ridership, there is not enough evidence about the ridership trend.

Conclusions

In this study, new evidence related to the impacts of implementing a contraflow bus lane on bus

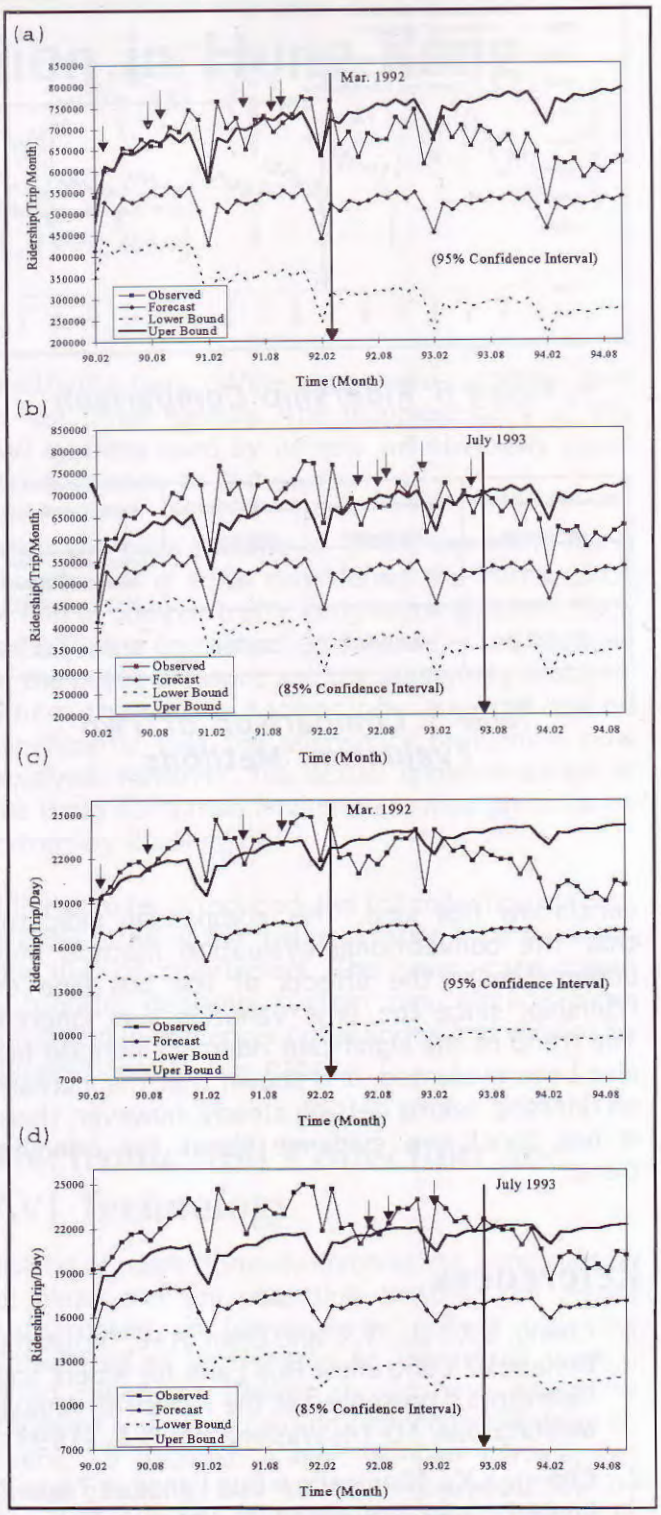

*Figure 7: **Comparison between Observed and Forecast Data***

ridership are presented. Box-Jenkins modelling techniques are used to forecast the ridership that would have resulted if the contraflow lane was not implemented. Comparison between the forecast and actually observed ridership is conducted.

Results of the analysis indicate that the ridership of the bus line assessed in this study increased about 28.5 percent after implementation of the

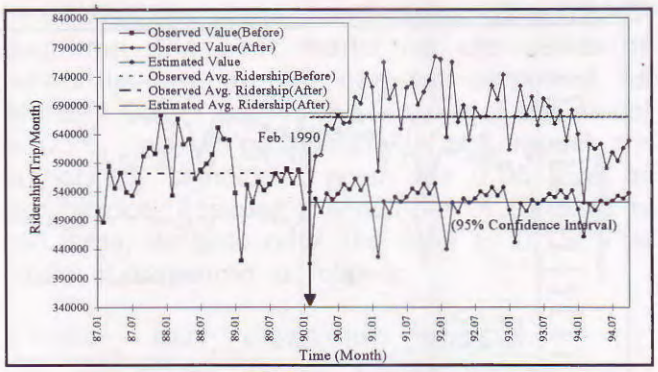

Figure 8: Ridership Comparison

Ridership Before Event (trips/month)	Ridership After Event (trips/month)	Estimated Ridership (trips/month)	AverageGrowth Rate	
P	A	E	Conventional Method (A-P)/P	New Method (A-E)/E
571553.3	669198.6	520714.6	17.1%	28.5%

Table 3: Comparison of Two Evaluation Methods

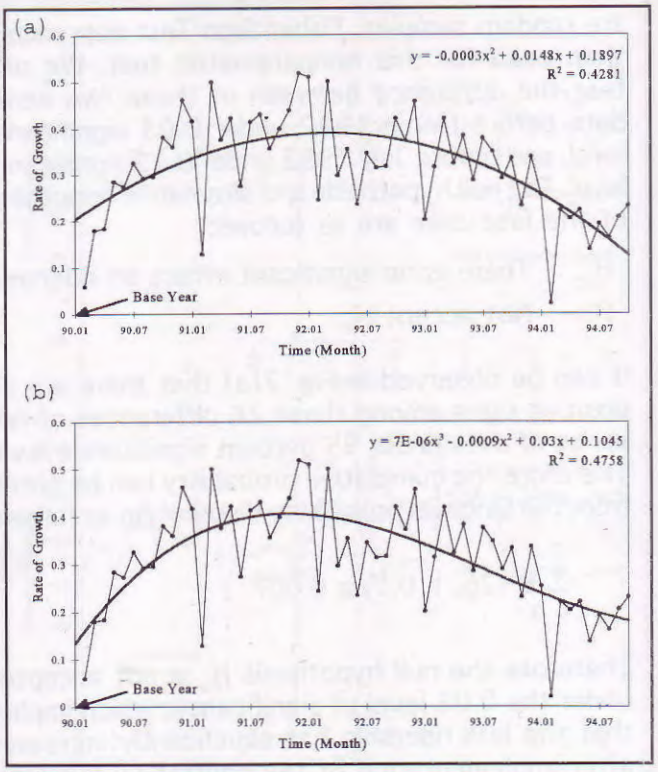

Figure 9: The Growth Rate Trend

contraflow bus lane. This comparison indicates that the conventional evaluation method may underestimate the effects of the bus lane on ridership, since the time variation was ignored. The trend of the significant ridership increase has also been evaluated. It is shown that the increase on ridership seems getting steady, however, there is not conclusive evidence about the ridership trend.

References

1. Chang, S.K., Lin, Y.S. and Chen, H.H., "Potential Benefit of Contraflow Bus Lane for Riders and Operators," presented at the 72nd TRB Annual Meeting, Jan. 10-14, Washington, D. C. (1993).
2. Chang, S.K., "Contraflow Bus Lanes in Taipei," invited paper presented at the 6th National Conference on High Occupancy Vehicle Systems, Transportation Research Board, October 25-28, Ottawa, Canada (1992).
3. Chang, S.K. and Chen, H.H., "Effects of Contraflow Bus Lane on Ridership," Compendium of Technical Papers, 63rd Annual Meeting, Institute of Transportation, The Hague, The Netherlands (1993).
4. Considine, J. J. and Narayan, J, "Assessment of the Impact of Changes in Transit Systems Using Intervention Analysis," Transportation Research, Vol. 22B, No. 1: 55-67 (1988).
5. Taipei Bus Management Center, Reports of Management Condition and Performance, January 1987 - October 1994 (1987-1994).
6. Anderson, T. W., et al., "The Statistical Analysis of Time Series," John Wiley and Sons (1972).
7. Bowerman, B. L. and O'Connell, R. T., "Forecasting and Time Series: An Applied Approach," North Scituate, Massachusetts (1979).
8. Box, G.E.P. and Jenkins, G.M., "Time Series Analysis Forecasting and Control," Holden-Day, San Francisco (1970).

Electronic Toll Collection in Hong Kong

by
W.K. Lam
Ph.D., C.Eng., MHKIE, Hong Kong

Abstract

The use of Automatic Vehicle Identification (AVI) technology in Electronic Toll Collection (ETC) is widely recognised for its capability to improve the capacity of the toll system. Three toll roads in Hong Kong are now installed with AVI system, and the others are considering the feasibility of its introduction. Two new toll crossings have already specified the use of AVI system in the toll collection system configuration. This paper describes the operational characteristics of AVI and its application in the current electronic toll collection system in Hong Kong.

Introduction

Road pricing has been attracting interests from many countries not only because of its potential to combat traffic congestion but also its ability to generate revenue. Closely associated with electronic road pricing is the technology of electronic toll collection (ETC) involving the use of automatic vehicle identification (AVI) for cashless toll transactions. This paper describes the operational characteristics of AVI and the electronic toll collection systems currently used in Hong Kong.

Following the current upsurge in economic development in many Asian countries, their governments are keen to involve the private sectors in developing highway infrastructure to serve the mobility demand as a result of rapid economic development. The fund originally reserved for highway improvement programme can be relocated for other areas requiring equally urgent investment. Because of the operational benefit of AVI in electronic toll collection, operators of many new and existing toll roads are expressing interest in such technology.

In Hong Kong, there are seven existing toll roads, with three new ones to be completed in the next few years. Currently, only three of them are now operating with AVI. Others are also considering the possibility of its introduction, but possibly with different AVI system. For example, one tunnel is now preparing a trial in late 1994, but with read/write tags, different to those currently used in the three tunnels. The incompatibility of the AVI systems used by tunnels will obviously cause inconvenience to the users.

After the pilot scheme in 1985, the Hong Kong Government is again considering the introduction of ERP to combat traffic congestion problem. Back in 1985, the original scheme was rejected because of the public pressure and the anonymity problem. Since then, the technology has advanced significantly that the anonymity problem is now resolved. However, the actual implementation in the Hong Kong road environment may prove to be extremely challenging.

If ERP is to be introduced, the toll collection method is likely to be of the 3rd generation type involving the use of smart-card. The smart-card based automatic debiting system has already been described in numerous publications and will not be detailed here in this paper.

Electronic Toll Collection and AVI Technology

Tolling of roads normally involves the construction of plaza and toll collection booths. Toll plazas constructed on highways to collect tolls are considered as bottlenecks to the traffic flow. A good toll plaza design should have adequate capacity and avoid causing unacceptable delay to users. To maintain a high level of service, toll plaza capacity has to be improved, say by increasing the number of toll booths, in order to meet the increasing traffic demand. However, constructing new toll booths is costly and requires land space which is often difficult to provide especially in densely populated cities such as Hong Kong. Electronic toll collection technology involving the use of automatic vehicle identification (AVI) is therefore becoming popular because of its capability in increasing the toll lane capacity without requiring additional land space.

AVI works by using wireless communications between a tag (transponder) mounted on a vehicle

and a sensor located at the road side. When a vehicle equipped with an AVI tag approaches the toll lane, communications will then be activated between the tag and the transceiver mounted at the road-side. Toll transaction is then made without the vehicles requiring to stop.

The use of AVI system not only improves the capacity of toll plaza, but also minimises the usage of land and operating costs. In addition, traffic not requiring to stop at the toll plaza will improve the environment as a result of reduction in vehicle emissions.

The AVI Tag Technology

The communications between the tag and the transceiver can be one-way (read only) or two-way (read/write). For the read-only type tag, typical information stored on tag include site code, account number, users number and vehicle class. However, the transaction details such as credit balance and time of transactions are held in the central system. With the read/write tags, transaction details and credit balance are stored in the tags themselves, i.e. the system has the ability to write new information such as new credit balance onto the tags as well.

About 90% of the tags being used today are the read-only tags, which can be considered as the first generation of AVI transponder device for non-stop payment system. The system currently used in Hong Kong is of the first generation type. The second generation is the read/write tags which are now being employed in many new installations of electronic toll collection facilities.

In the near future, the 3rd generation of AVI transponder will be in the form of smart-card (not a tag) and will have the capability to interact and communicate with the drivers. The technology is still being developed and there have been trials to test its application on non-stop tolling in multi-lane roadway without toll plaza configuration. Singapore is actively pursuing this course of automatic debiting system with an aim of full implementation in 1997 to replace the existing Area Licencing Scheme.

AVI Communications Technologies

The AVI system used in the pilot road pricing scheme in Hong Kong in the mid-eighties [Catling, 1985] was essentially based on inductive loops buried underneath the road and a bulky electronic circuitry box mounted underneath the vehicles. Since then, the AVI technology has advanced significantly. Burying cables and bulky circuitry box mounted in the vehicles will no longer be required in today's remote identification technology.

The wireless communication technique between the tag and the interrogator (the transceiver) available for automatic vehicle identification include:

- inductive identification systems
- infra-red systems
- radio frequency systems such as microwave
- optical character recognition system
- bar coding system
- surface acoustical wave

The bar-code system used in Bay Habour Island of Miami and the inductive system used in Hong Kong's pilot project represent the early version of AVI system.

The above AVI transmission media have their pros and cons. The microwave-based is however more widely used than other technologies. This is because of its high reliability, speed and tolerance to environment. However, its resistance to lane to lane interference may be low and thus requiring careful calibration on site.

The microwave-based AVI system could have two basic types of transmission characteristics depending on the type of tags being used.

- Active microwave system
- Passive microwave system

With active microwave vehicle tag system, the tag has a power source which enables it to generate its own microwave signals. The reliability and operating distance are greatly enhanced because of stronger signals returning to the transceiver.

On the other hand, the passive tags may or may not require a power source. There are many existing AVI systems employment tags which modulate the incoming microwave signal received and then reflect it back onto the transceiver for subsequent processing. The tag battery only requires to provide energy for information storage and signal modulation and therefore possesses longer operating life.

The main advantages and disadvantages of the active and passive systems can be summarised below.

Most of the AVI systems employed for electronic toll collection are based on the passive microwave

technology, such as those used in Hong Kong, the Dartford and Mersey in the UK [Morton and Lam, 1994]. The radio frequency being used in these systems is 2.45 GHz, although the European Unions have already standardised the AVI microwave frequency as 5.8 GHz.

The Operating Characteristics of AVI

An AVI system typically consists of a communication system on the road side and an ID tag mounted in the vehicle. A typical installation at a toll lane is shown in Figure 1. Reinforcement camera is also employed nowadays to record the details of vehicles violating the system. The existing toll configuration in Hong Kong does not employ a barrier at the toll booth.

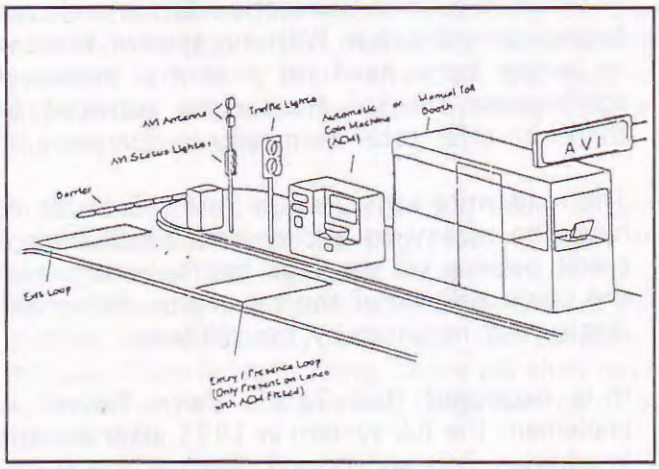

Figure 1: Typical installation at an AVI Toll Lane

The AVI tag is slightly smaller than the size of a 3.5" computer floppy disk but of about 10 to 12 mm thick. The coding in a tag is unique to each vehicle, and a tag issued for cars can not be transferred to trucks which should be paying higher toll charge.

In the operation of an AVI system with passive communication tags such as those used in Hong Kong, the antenna transmits microwave signal continuously to search for presence of tags. An AVI-equipped vehicle approaches the toll booth and reaches the detection zone, the tag in the vehicle is energised and responded to the interrogating signal back to the antenna. The information is then being fed to the computer for validation check and subsequent debiting processing. The AVI status light at the booth side will turn green if the account is valid and in credit. The vehicles can then proceed to go and an appropriate toll charge will be deducted from the account. This process could take place when the vehicle is still moving forward at a speed.

If the account is low in credit, the AVI status will turn amber to warn the driver to renew credit next time, but the vehicle is still allowed to proceed. When the account is not in credit, as indicated by a red AVI status light, the vehicle can still pass the toll booth but has to renew the credit at the administration building within a certain period of time. Otherwise, enforcement by summon will be issued.

The AVI tags issued to each vehicle are not transferable. However, there is not an automatic vehicle classification system which could automatically verify the vehicle type information on the tag. The current system has to rely on the occasional manual verification, although the new system in Tate's Cairn Tunnel will have the read/write tags inscribed with the shape of the vehicle class to assist the verification process.

The Improvement in Toll Capacity due to AVI

AVI can increase the toll capacity by means of cashless toll collection and thus reducing the time spent at the toll booths. It has been reported that the inter-vehicle headways at an AVI toll booth (with barrier) has been observed to reduce by more than 40 per cent [Morton & Lam, 1994].

In Hong Kong, all existing toll systems are not configured with barriers. It has been reported that the normal capacity is approximately 600 veh/h, and in the dedicated AVI toll lane (channelised) the capacity is doubled to reach approximately 1200 veh/h, similar to that observed in the USA.

For a toll lane with barrier such as those installed at the Dartford Crossing in the UK, the capacity can be increased by some 80% from 470 veh/h to 860 veh/h.

The potential capacity achieved by AVI as described above is for conventional toll plaza configuration with lane channelisation. For express AVI lanes separated from the toll plaza, or the non-stop multi-lane toll system under trial in Singapore [Lew, 1994], the capacity then depends on the freeway lane capacity, e.g. 1800 veh/h. Figure 2 summarises the capacity of various types of toll lane.

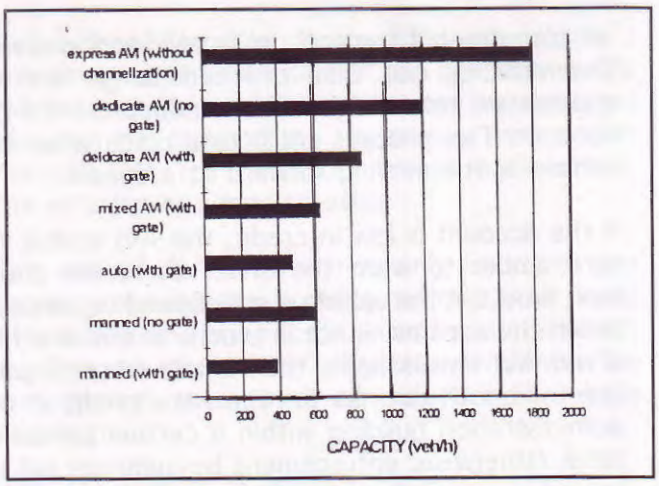

*Figure 2: **Capacity of Different Toll Lanes***

The Toll System in Hong Kong

There are currently seven toll crossings in Hong Kong, as illustrated in Figure 3. Three additional toll roads will also be in operation in the next few year.

Cross Harbour Tunnel and Eastern Harbour Crossing are the only two links across the Victoria Harbour serving the traffic between the Kowloon peninsula and the Hong Kong Island. They are both twin two-lane tunnels and are already at capacity. A third crossing, the Western Harbour Crossing, is programmed to complete in mid-1996.

Out of the existing seven toll tunnels, three are now installed with passive microwave-based AVI system using the Autopass's AMTECH read-only tags. Autopass Co. Ltd. was set up by Cross harbour Tunnel and the AMTECH of the USA and is responsible for the administration of the AVI system on behalf of these tunnels.

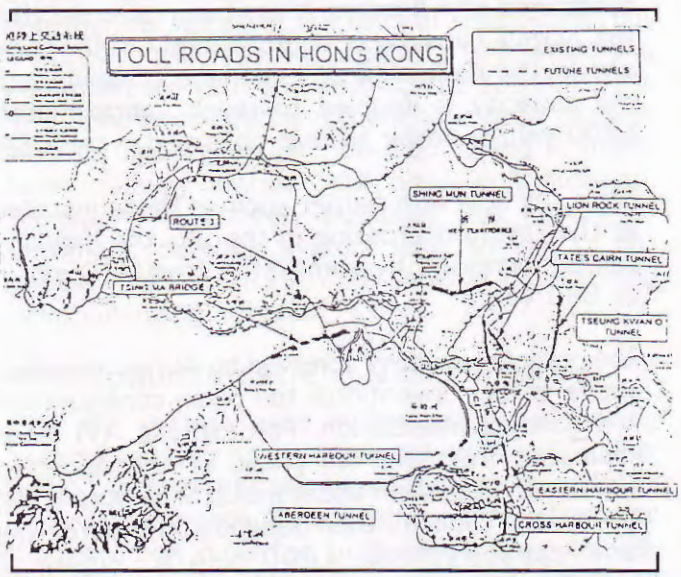

*Figure 3: **The Toll Roads in Hong Kong***

Cross Harbour Tunnel was the first to introduce AVI toll collection in Hong Kong in 1993. This was then followed by the Aberdeen Tunnel and the Lion Rock Tunnel in late 1994.

Of the remaining four toll tunnels, Tate's Cairn Tunnel and Eastern Harbour Crossing are also suffering from sever traffic congestion in peak hours and are now considering the introduction of AVI. In fact, Tate's Cairn Tunnel has already begun to install a different AVI system employing read/write tags for trial in late 1994. These tags are the Premid (Programmable Remote Identification) tags by Saab-scania Combitech AB of Sweden. This AVI system will enable the writing of new information such as transaction details and credit balance onto the tags. With this system, there will no longer be a need for a central system to administrate the toll transaction activities and therefore offer total anonymity to the users.

The read/write tags used in Tate's Cairn do not have the facility to display information such as credit balance on the tags themselves. Instead, the credit balance of the tag will be shown on a display unit mounted by the toll lane.

It is expected that Tate's Cairn Tunnel will implement the full system in 1995 after the trial. In addition, it is understood that the AVI system for the future Western Harbour Crossing and Lantau Fixed Crossing is also considering the use of read/write tags. It is more than likely that there will be two separate and incompatible toll collection systems in operation in Hong Kong.

If the Hong Kong Government succeeds in introducing ERP in the coming years, automatic debiting technology using smart cards will be used. This will add another dimension of system incompatibility onto the future toll operation environment in Hong Kong. Without system standardisation, as far as the users are concerned, they may end up with possibility several toll transaction devices (tags and smart-card as well) in their vehicles.

Conclusions

Road pricing or tolling of existing/new roads is becoming increasingly popular in many countries, irrespective of its usage as a means to combat

congestion or to generate revenue. The use of automatic vehicle identification (AVI) technology in automatic toll collection is recognised worldwide for its potential to improve toll capacity, and many such systems have been implemented in recent years.

All the existing toll roads in Hong Kong are configured with conventional toll plaza and the application of AVI system in Hong Kong (without barrier) has been found to increase the toll capacity by about 100% from 600 veh/h (manual) to approximately 1200 veh/h. The benefit of AVI not only improves the capacity, but also reduces the operating cost and land space for toll plaza.

Three tunnels in Hong Kong are installed with AVI system employing read-only tags. Other tunnels are taking steps to improve the toll capacity. One tunnel is now progressing to implement a different AVI system using read/write tags. Two of the three new toll roads are also considering the use of read/write tags as part of their AVI toll collection systems. It is likely that more than one type of AVI system will be in operation in Hong Kong in the next few years.

In addition, electronic road pricing using smart-card based automatic debiting system is now on the agenda of the Transport Department of Hong Kong. This may yet add another dimension of the system incompatibility onto the toll collection infrastructure in Hong Kong. Users will then have to install several toll devices (tags and card) in the vehicles.

Finally, as the transport infrastructure is increasing the use of AVI technology, it is naturally logical to consider the standardisation and integration of various AVI systems in Hong Kong. Moreover, as common-stored value smart card is now being developed in Hong Kong for fee paying activities in car parking, MRT, buses and ferries, etc, the integration with the debiting system for the electronic road pricing, if approved, will be beneficial.

References

1. Catling, I., and B.J. Harbord, Hong Kong: The Technology, Traffic Engineering & Control, Vol 26, No. 12, Dec 1985.
2. Lew, Y.D. et al., Electronic Road Pricing in Singapore - Demonstration Project, Proceedings of the International Conference on Advanced International Conference on Advanced Technologies in Transportation and Traffic Management, Singapore, May 1994, pp 113-120.
3. Morton, T.W. and W.K. Lam, The Effect of Automatic Vehicle Identification on the Toll Capacity at Dartford River Crossing, Traffic Engineering & Control, May 1994.

Simultaneous Measurement of Thermal Conductivity and Thermal Diffusivity of Pavement Materials

by
Dr. Low Boon-Hwee
Technical Manager
Eng Seng Construction (Pte) Ltd., Singapore

and

Dr. Fwa Tien-Fang — Associate Professor
Dr. Tan Siew-Ann — Senior Lecturer
Department of Civil Engineering
National University of Singapore, Singapore

Abstract

The paper describes a simple laboratory method for the measurement of thermal properties of highway and airfield pavement materials such as bituminous mixes and portland cement concrete. The technique involved simultaneous measurement of thermal conductivity (k) and thermal diffusivity (α) from single heating experiment of a thin slab based on transient heat conduction theory. The reduction method involved an analytical technique to fit the inflection point on the temperature -$\sqrt{t}$ history plot to the theoretical inflation point. The values of k and α obtained by this procedure compares favourably with reported literature data and give support to the validity of the procedure.

Introduction

The performance of pavement materials such as bituminous mixture and portland cement concrete are influenced to a certain extent by temperature. For instance, the compactness, stability, and viscosity of bituminous mixes is found to be dependent on their mixing, compaction and service temperatures. Hence the thermal properties of these pavement materials are important in pavement design. Thermal stresses induced in the concrete and bituminous pavement are one of the important consideration in the development of a structural or mechanistic method of design for pavements.

In order to study the thermal behaviour of pavements materials, their thermal properties must be known. The thermal properties of interest are the thermal conductivity (k), thermal diffusivity (α) and volumetric specific heat (c_p). The usual way to determine these properties is to measure k, and α separately, that is to measure k by steady-state method and α by transient heat conduction methods. The third property, c_p can than be computed as $k/p\alpha$ if the density p is known.

In this paper, a method is proposed to measure both k and α simultaneously from a single experiment based on the theory of transient heating of a thin slab subjected to external forced convection. The theory enables the non-dimensional temperature-time history for the mid-plane of the slab to be obtained for any values of k and α. The data reduction method proposed uses an analytical technique to fit the inflection point on the temperature -$\sqrt{t}$ plot to its corresponding theoretical inflection point, thus arriving at the values of k and α to obtain the best fit.

Theory of Transient Heating of Thin Slab

The theory that describes the temperature response of a plane wall with an initial temperature T_i after it is suddenly immersed in a fluid medium of temperature T_f, where T_f is greater than T_i, has been discussed in Incropera and Dewitt [1990] and Low [1994]. The temperature-time history at the midplane of a plane wall is expressed as

$$\theta^*_p = \sum_{n=1}^{\infty} C_n \exp(-\zeta_n^2 Fo) \qquad (1)$$

where the mid-plane normalized temperature is $\theta^* = (T-T_f)/(T_i-T_f)$, Fo is the Fourier Number, and the coefficient $C_n = 4\sin\zeta_n/(2\zeta_n + \sin[2\zeta_n])$, and the discrete values (eignevalues of the ζ_n are the

positive roots of the transcendental equation $\zeta_n \tan\zeta_n = Bi$.

In order to compare the theory with experimental results, an estimate of the Biot number is required. For the case of a flat plate in parallel air flow with a velocity *u*, the average heat convection transfer coefficient $\bar{h}$ can be obtained as follows [Churchill and Chu 1975]:

$$\bar{h} = \frac{\overline{Nu_L} k_a}{L} \qquad (2)$$

where k_a is the thermal conductivity of air, L is the characteristic length of plate (equal to the width of plate), and $\overline{Nu_L}$ is the average Nusselt number for the flat plate for laminar flow which is express as

$$\overline{Nu_L} = 0.664 Re_L^{1/2} Pr^{1/3} \qquad (3)$$

where Re_L is the Reynolds number equals to uL/ν, u is the air velocity, ν is the viscosity of air at film temperature $(T_i + T_f)/2$, and Pr is the Prandtl number (≥ 0.6).

To apply the theory to a square slab of dimension 2L x 2L x 2d, it is necessary to determine the limiting ratio of d/L that would give identical temperature response at its centre-point to that at the mid-plane of a plane wall. The expression for the temperature history at the centre-point of a square slab is given by the product of the solutions of three plane wall problems taken at x = 0, y = 0, and z = 0,

$$\theta(x,y,z,t) = \theta_p(x,t).\theta_p(y,t).\theta_p(z,t) \qquad (4)$$

From Equations (1) and (4), the specific solutions for d/L of 0, 0.2, 0.4 and 0.6 are determined and plotted as θ^* versus Fo in Figure 1. It is obvious

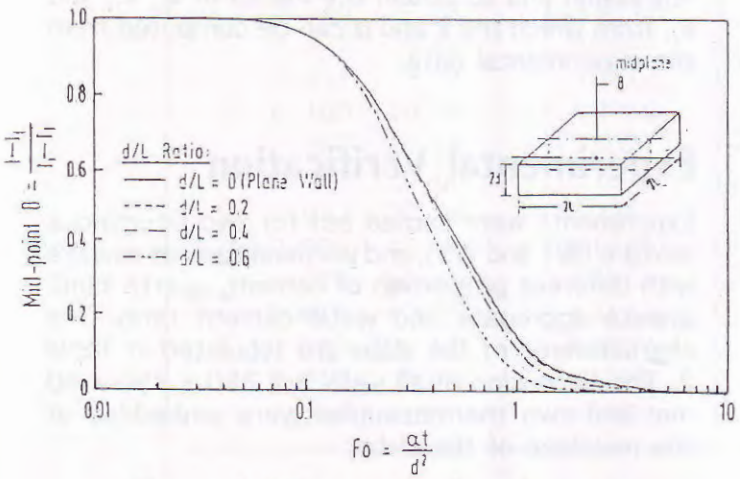

*Figure 1: **Theoretical mid-point temperature history of square slab for various d/L ratios.***

that up to d/L of 0.2, the temperature history at the centre-point of the square slab coincides with that of a plane wall (d/L = 0). for d/L greater than 0.2, the deviation from the plane wall behaviour becomes progressively larger. Thus, from the experimental view point, it is adequate to adopt a thin slab with a d/L less than 0.2 to ensure one dimensional heat flow across the centre-point of the slab.

Data Reduction Method

The plane wall solution of Equation (1) is used to obtain the solutions of the temperature time history for various combinations of Biot numbers for the case of a thin slab. The results are presented in Figure 2 as a family of θ^* versus $\sqrt{Fo}$ curves which are strongly dependent on the value of Bi. the concept of curve fitting in this scheme is to fit the inflection point of an experimental temperature-time history to the analytical inflection point. At each inflection point, a linear equation of a line tangent to the curve at the inflection point can be obtained if the gradient and intercept are known. The equation for the tangent line is

$$\theta^* = M\sqrt{Fo} + C \qquad (5a)$$

Substitute for $Fo = \alpha t/d^2$, Equation (5a) becomes

$$\theta^* = M\sqrt{\frac{\alpha}{d^2}}\sqrt{t} + C \qquad (5b)$$

where M is the theoretical slope, and C is the theoretical intercept of the straight line tangent through the inflection point.

From the experimental data, a similar inflection point can be determined and the linear equation through this point is

$$\theta^* = m\sqrt{t} + c \qquad (6)$$

where m is the experimental slope, and c is the experimental intercept at inflection point.

If the experiment is performed according to the boundary condidtions of the theoretical solution, the inflection points from both experimental and analytical solutions must be identical. thus, by equating the slopes and intercepts of Equations (5b) and (6):

$$m = M\sqrt{\frac{\alpha}{d^2}} \quad \text{or} \quad \alpha = \left(\frac{m}{M}d\right)^2 \qquad (7)$$

and

$$c = C \qquad (8)$$

From Figure 2, it is obvious that the theoretical C are directly related to Biot numbers or (hd/k) and it can be theoretically derived as functions of Bi.

From experiment, c can be determined directly. Since c = C, the Bi number for the material tested can be identified and hence the thermal conductivity, k determined as:

$$k = \frac{\bar{h}d}{Bi} \qquad (9)$$

Similarly, the theoretical M is the function of Bi number as well. Once the Bi number is identified, M can be determined and hence the value of α can be obtained from Equation (7).

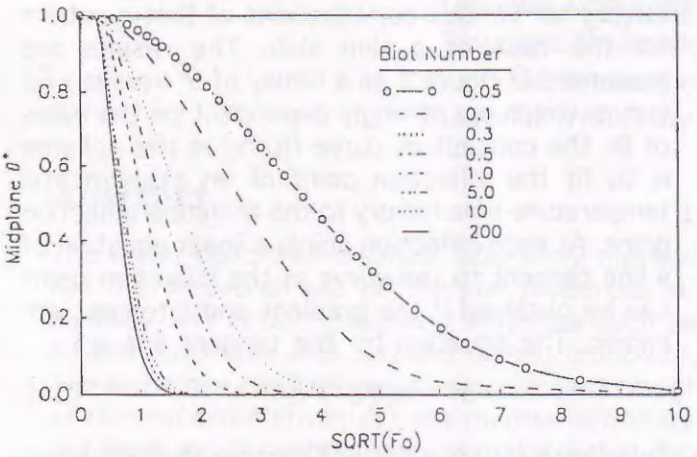

Figure 2: Mid-plane temperature vs $\sqrt{Fo}$ for range of Bi number.

Determination of M and C

The temperature gradient with respect to $\sqrt{Fo}$ can be expressed by using chain rule and differentiation Equation (1) as

$$\frac{d\theta^*}{d\sqrt{Fo}} = \frac{d\theta^*}{dFo} \cdot \frac{dFo}{d\sqrt{Fo}} \qquad (10a)$$

where $$\frac{d\theta^*}{dFo} = \sum_{n=1}^{\infty} -\zeta_n^2 C_n \exp(-\zeta_n^2 Fo) \qquad (10b)$$

and $$\frac{dFo}{d\sqrt{Fo}} = 2\sqrt{Fo} \qquad (10c)$$

Hence the temperature gradient at the inflection point (M) is given by

$$M = \frac{d\theta^*}{d\sqrt{Fo}} = 2\sqrt{Fo} \sum_{n=1}^{\infty} -\zeta_n^2 C_n \exp(-\zeta_n^2 Fo) \qquad (11)$$

In order to determine the inflection point, Equation (11) is differentiated a second time,

$$\frac{d^2\theta^*}{d\sqrt{Fo}^2} = 2\sum_{n=1}^{\infty} -\zeta_n^2 C_n \exp(-\zeta_n^2 Fo) + 4Fo\sum_{n=1}^{\infty} \zeta_n^4 C_n \exp(-\zeta_n^2 Fo) \qquad (12)$$

At the inflection point, equation (12) is equal zero and the corresponding slope, M at this point is minimum. By similar procedures, the inflection points, its slopes (M) and intercepts (C) are determined for various Bi reanging from 0.02 to 9999 and tabulated in Table 1.

Determination of m and c

To identify the exact inflection point directly from the experimental temperature-time data would be difficult. One way is to determine a polynomial equation that can describe the experiment data. A preliminary study shows that a polynomial equation of third order is good enough to describe the curve at the θ^* range of interest, from 0.5 to 0.7. The polynomial equation is expressed as

$$\theta^* = a_0 + a_1\sqrt{t} + a_2(\sqrt{t})^2 + a_3(\sqrt{t})^3 \qquad (13)$$

Differentiating equation (13) with respect to $\sqrt{t}$ will give the temperature gradient, m as

$$m = \frac{d\theta^*}{d\sqrt{t}} = a_1 + 2a_2\sqrt{t} + 3a_3(\sqrt{t})^2 \qquad (14)$$

To determine the inflection point, equation (14) is differentiated a second time which leads to

$$\frac{d^2\theta^*}{d\sqrt{t}^2} = 2a_2 + 6a_3\sqrt{t} \qquad (15)$$

At the inflection point, equation (15) is equal to zero, from which $\sqrt{t}$ at the inflection point is determined. By substituting $\sqrt{t}$ from equation (15) into equations (13) and (14), θ^* and m at the inflection point are determined. The intercept, c can then be evaluated from equation (6) by substituting for the values of θ^* and $\sqrt{t}$ at the inflection point. A computer programme was written using Lotus 123 to perform the polynomial regression and to obtain the values of a_o, a_1, and a_3, from which the k and α can be computed from the experimental data.

Experimental Verification

Experiments were carried out for two bituminous mixture (W1 and W3), and portland cement mixture with different proportion of cement, quartz sand, granite aggregate and water-cement ratio. The characteristic of the slabs are tabulated in Table 2. The dimension of all slabs are 250 x 250 x 40 mm and two thermocouples were embedded at the midplane of the slabs.

Table 1: Theoretical M and C at Inflection Points

1/Bi	Bi	M	C	$\sqrt{F}$	0
50.000	0.02	-0.12134	1.217079	5.014941	0.608539
10.000	0.10	-0.27114	1.232590	2.272924	0.616295
6.667	0.15	-0.32637	1.240947	1.901080	0.620473
5.000	0.20	-0.38277	1.250765	1.633795	0.625382
4.000	0.25	-0.42486	1.258857	1.481472	0.629428
3.333	0.30	-0.46774	1.267707	1.355130	0.633853
2.857	0.35	-0.50275	1.275347	1.268355	0.637672
2.500	0.40	-0.53835	1.283455	1.192036	0.641719
2.000	0.50	-0.59967	1.298131	1.082498	0.648986
1.667	0.60	-0.65399	1.311750	1.003398	0.655530
1.429	0.70	-0.70286	1.324376	0.943494	0.661227
1.250	0.80	-0.74713	1.336023	0.896794	0.665999
1.111	0.90	-0.78768	1.346796	0.859356	0.669890
1.000	1.00	-0.82485	1.356697	0.828899	0.672979
0.833	1.20	-0.88348	1.372276	0.787075	0.676906
0.714	1.40	-0.94297	1.387880	0.750949	0.679753
0.667	1.50	-0.97297	1.395625	0.734677	0.680800
0.625	1.60	-0.99389	1.400976	0.723957	0.681442
0.556	1.80	-1.03589	1.411555	0.703833	0.682455
0.500	2.00	-1.07808	1.421915	0.685262	0.683142
0.455	2.20	-1.10573	1.428584	0.673770	0.683572
0.417	2.40	-1.13343	1.435128	0.662777	0.683913
0.385	2.60	-1.16116	1.441528	0.652242	0.684169
0.357	2.80	-1.18889	1.447761	0.642128	0.684338
0.333	3.00	-1.21660	1.453804	0.632403	0.684420
0.313	3.20	-1.23125	1.456983	0.627316	0.684595
0.286	3.50	-1.25322	1.461652	0.619852	0.684835
0.250	4.00	-1.30332	1.471678	0.603624	0.684962
0.222	4.50	-1.32896	1.476642	0.595484	0.685263
0.200	5.00	-1.36240	1.482710	0.585212	0.685411
0.167	6.00	-1.40523	1.490014	0.572298	0.685798
0.143	7.00	-1.43741	1.495075	0.562765	0.686150
0.125	8.00	-1.46255	1.498743	0.555393	0.686451
0.111	9.00	-1.48272	1.501480	0.549520	0.686695
0.100	10.00	-1.49916	1.503575	0.544745	0.686912
0.067	15.00	-1.55027	1.509171	0.529947	0.687609
0.050	20.00	-1.57676	1.511442	0.522265	0.687955
0.033	30.00	-1.60382	1.513228	0.514380	0.688251
0.025	40.00	-1.61745	1.513905	0.510385	0.688382
0.020	50.00	-1.62568	1.514233	0.507960	0.688449
0.017	60.00	-1.63123	1.514411	0.506322	0.688479
0.013	80.00	-1.63807	1.514601	0.504292	0.688529
0.010	100.0	-1.64218	1.514694	0.503070	0.688558
0.000	9999.	-1.65880	1.514848	0.498107	0.688582

Table 2: ***Summary of k and α measured.***

Material	Density kg/cm³	*k* W/mK	α x 10^{7} m^2/s
Bituminous mix (W1)	2203	1.37	6.30
Bituminous mix (W3)	2275	1.44	6.13
Concrete (2:3:4:1)	2353	1.11	14.59
Cement/ sand (2:3:0:1)	2114	1.19	6.47
cement/ aggregate (2:0:4:1)	2332	1.34	6.21
hardened cement (2:0:0:1)	1974	0.99	4.00

Figure 3 shows the schematic diagram of the vertical slab experiment. The chamber used is a high precision temperature chamber that can control temperature stability and uniformity up to 0.5°C. The slab is initially place in the chamber with temperature set at T_i = 25°C, until equilibrium is reached. Subsequently, the temperature of the chamber is reset to 60°C. The temperature at the midplane as measured by thermocouple A and B are recorded immediately when the chamber temperature reaches 60°C, by an automatic data recording system at every 10 seconds intervals subsequently.

Figure 4 shows a typical temperature-time history for the vertical slab experiment. Polynomial regression was done at θ* range of 0.5-0.7 to determine the inflection point and the experimental m and c using equations (6) and (13)-(15). k and α can be calculated from equation (9) and (7) respectively, and was found to be 1.33 W/mK and 5.47 x 10^{-7} m^2/s. With the values of k and α determined, the theoretical temperature-time history is obtained and superimposed onto the experimental data as in Figure 5. Undoubtedly, the theory and experiment agree with one another very well thus validating the technique for curve fitting to determine simultaneously the values of k and α from the experimental data.

The thermal conductivities and diffusivities obtained by the proposed method compares favourably with those reported elsewhere. O'Blenis [1954] measured k and α in situ for highway pavements with a range of 0.85-2.32 W/mK and 4.61-11.98 x 10^{-7} m^2/s, respectively. These values compared favourably with the values measured as summarised in Table 2.

Rhodes [1978] and Zoldners [1971] reported the thermal conductivity of saturated hardened portland cement with water-cement ratio of 0.3 to 0.6 at normal air temperature between 0.8 to 1.2 W/mK which agrees with our measured values of 0.99 W/mK for a neat cement slab of w/c of 0.5. Rhodes [1978] reported diffusivities of neat hardened cement pastes ranging from 3.3-4.0 x 10^{-7} m^2/s which compared very well with our measured values of 4.0 x 10^{-7} m^2/s.

Conclusion

From the plane wall theory, a simple data reduction to determine thermal conductivity and diffusivity simultaneously were proposed. The technique involved an analytical curve fitting procedure to

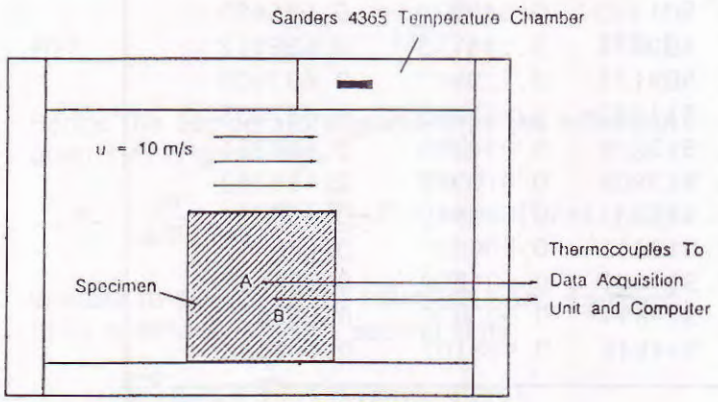

Figure 3: ***Slab specimen in transient conduction experiment set up.***

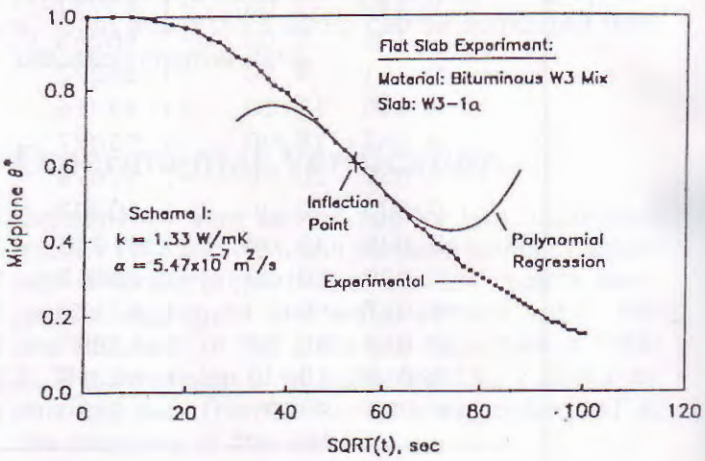

Figure 4: ***Polynomial regressifon of experimental data.***

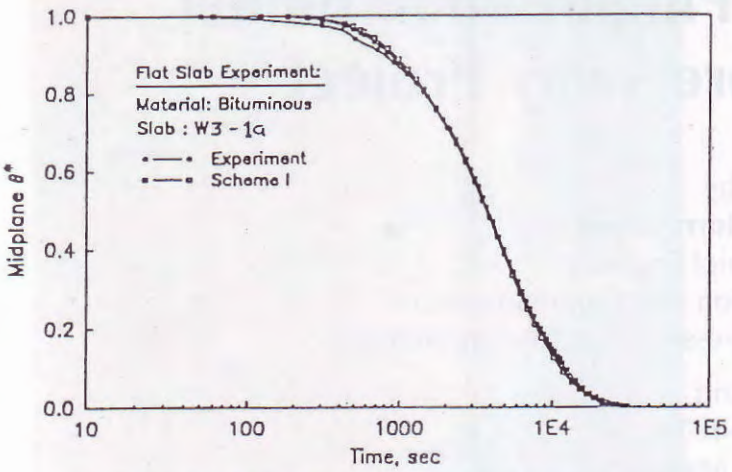

*Figure 5: **Prediction of temperature history using k and a measured.***

fit the inflection point on the experiment temperature-$\sqrt{t}$ curve and the theoretical inflection point. The experiment can be done with thin slab in a uniform horizontal flow temperature chamber.

Comparison with other reported values of k and α indicated that the measured values are well within the common range of k and α. The methods proposed are inexpensive and simple, thus making the approach a highly attractive and method for the determination of k and α of pavement materials.

References

1. Churchill, S.W. and Chu, H.H.S. [1975], "Correlating Equations for Laminar and Turbulent Free Convention from a Vertical Plate", International Journal of Heat and Mass Transfer, Vol. 18, pp. 13-23.
2. Incropera, F.P. and Dewitt, D.P. [1989], Fundamentals of Heat and Mass Transfer, 3rd Ed., John Wiley and Sons, New York.
3. Low Boon-Hwee, [1994], Laboratory Characterisation of Bituminous Mixtures for Pavements, Ph.D. Thesis, National University of Singapore.
4. O'Blenis, J.D. [1954], Thermal Properties of West Virginia Highway Materials, M.Sc. Thesis, West Virginia University.
5. Rhodes, J.A. [1978], "Thermal Properties of Concrete", ASTM STP 169B, pp. 242-261.
6. Zoldners, N.G. [1971], "Thermal Properties of Concrete Under Sustained Elevated Temperatures", ACI SP 25, pp. 1-31, Detroit, MI.

The Boring of the Pinglin Pilot Tunnel Taipei–Ilan Expressway Project

by
Dr. Lee Horng-Cheh
Deputy Chief Engineer
Ministry of Transportation and Communications
Taiwan Area National Expressway Engineering Bureau

and
Teh-Yi Yu
Project Manager
Sinotech Engineering Consultants, Inc.

Abstract

The 12.9 km long Pinglin Pilot Tunnel is one of the components of the Taipei-Ilan Expressway Project. The major purpose of the pilot tunnel is to explore the geology and to drain groundwater in advance along the route of the Pinglin main tunnels which will cross a complicated geological terrain in the first 3 km from the eastern portal and several major faults in other parts. A double shield TBM is being employed to drive the pilot tunnel. Since the beginning of the use of the machine in December 1992, there have been some serious problems. Several fractures have been encountered during the course of driving, causing much slowdown in the work progress. This paper reports on the methods that have been adopted to enable the machine to penetrate through these fractures.

The Project

The 30.8 km long Taipei-Ilan Expressway Project is located on the northeast mountainous terrain of Taiwan (Figure 1). The project is aimed at shortening the travel time between Taipei and Ilan from the current 2.5 hours to within 30 minutes.

Stretching through the mountainous terrain, the expressway consists of 5 tunnels with a total length of approximately 20 km. The 12.9 km twin tube Pinglin Tunnel is the longest and a key to the success of the project.

Major features of the Pinglin Tunnel:

- **Length:** 3 x 12.9 km (including the pilot tunnel)
- **Diameter:** 4.8 m for the pilot tunnel and 11.8 m for two main tunnels.
- **Gradient:** 1.255% ascent from Toucheng (east) to Pinglin.
- **Ventilation shafts:** 2 shafts each at 3 ventilation stations for fresh air and exhaust air respectively; distance between shafts, 50 m.
- **Air interchange stations:** 3 staggered with ventilation stations, for transferring air from one tunnel to another to achieve air quality balance.
- **Cross connections between main tunnels:** For pedestrians: 28 cross connections in all (one per 350 m), which also provide access from the main tunnels to the pilot tunnel for emergency personnel evacuation.

  For vehicles: 8 in all (one per 1,400 m), for emergency use by vehicles to enter east bound or west bound tunnel and for providing pedestrian access to the pilot tunnel.
- **Pilot tunnel:** Located between and parallel to the two main tunnels throughout their length for purposes of geological exploration and ground pretreatment, and for use as auxiliary access during main tunnel construction and as emergency access after completion of the expressway. The layout of the three tunnels is shown in Figure 2.
- **Cost:** USD 1 billion equivalent.

Geology

The entire length of the Pinglin Tunnel is located in the Hsuehshan Range geological sub-province of the Central Range geological province. This geological sub-province is underlain by folded Tertiary sedimentary rock formations, and

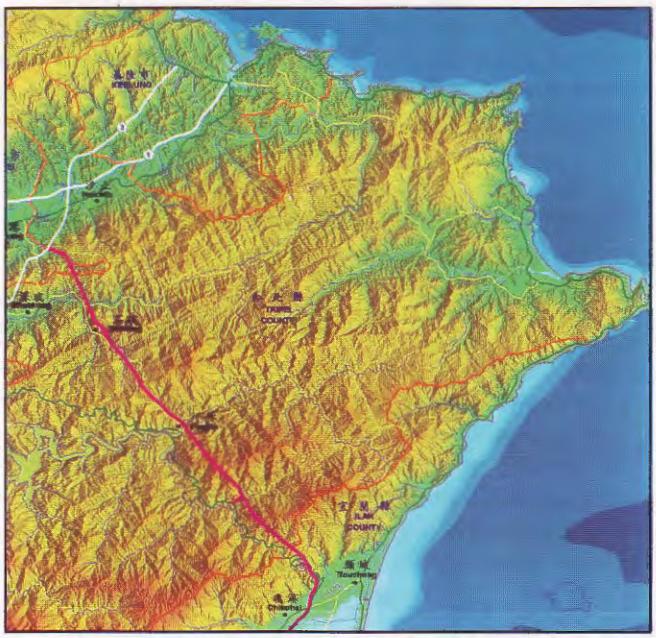

*Figure 1: **Taipei-Ilan Expressway***

*Figure 2: **Perspective of Pinglin Tunnel***

belongs to a fold-and-thrust structural belt. The sedimentary formations had been subjected to the Penglai Orogeny that commenced in Pliocene and continues to Recent. As a result of this structural process, the rock formations are folded and thrust faulted.

The major rock strata in the project area include:

- **Szeleng Sandstone:**

  This is the oldest rock formation in the project area. Outcrops of rocks of this formation occur mostly in the eastern half of the tunnel. The Szeleng Sandstone is composed of fine-grained sandstone and coarse to medium-grained quartz sandstone intercalated with carbonaceous shale. The rock mass between Chinying Fault and Shihpai Fault is poor and fractured. The Szeleng Sandstone may contain large quantities of groundwater. The uniaxial compressive strength of rock core is 800-2200 kg/cm^2.

- **Kankou Formation:**

  This formation is also limited in occurrence to the eastern half of the Pinglin Tunnel. The Kankou Formation is composed of thick, fractured argillite. Bedding planes of this argillite is poorly developed. There are occasional occurrences of siltstone beds. The rock mass is very poor and joints are well developed from the east portal to the Chinying Fault. Some of the sheared areas may contain large quantities of high pressure water which may trigger cave-in during excavation. The uniaxial compressive strength of rock core is 200-600 kg/cm^2.

- **Tsuku Formation:**

  Only sporadic outcrops of rocks of the Tsuku Formation occur in the project area. In the section covered by the Pinglin Tunnel, the occurrence of the Tsuku Sandstone was derived from plotting and extending outcrops both to the north and the south of the tunnel alignment. Rocks of the Tsuku Formation comprise gray, very fine sandstone or silt stone with argillite intercalations. The rock mass is fair to good, and there is little groundwater. The uniaxial compressive strength is 500-1000 kg/cm^2.

- **Tatungshan Formation:**

  Siltstone or alternation of argillite and fine sandstone; light gray, fine to medium-grained sandstone with intercalations of thin siltstone or argillite; argillite with occasional intercalations of thin siltstone beds; and dark gray siltstone or alternations of argillite and fine sandstone. Rock mass is fair to good, and this formation may contain little groundwater. The uniaxial compressive strength is 100-600 kg/cm^2.

- **Makang Formation:**

  The Makang formation occurs west of the Shihtsao Fault, or on the two flanks of the Yingtzulai Syncline on the Pinglin Tunnel profile. This formation can be divided into an upper and a lower member. The lower member is composed mainly of alternations of sandstone and shale; the upper member is mainly composed of many thick beds of sandstone. The rock mass is fair and the formation contains less groundwater. The uniaxial compressive strength is 400-900 kg/cm^2.

- **Fangchiao Formation:**

  The Fangchiao formation is widely spread on the ground surface. Most of the formation will

not be penetrated by the tunnel. The formation conformably overlies the Makang formation. It can be divided into an upper and a lower lithologic member. The lower member is mainly composed of alternations of sandstone and shale while the upper member is composed of thick-bedded sandstone. The rock mass is fair to good. The uniaxial compressive strength is 300-800 kg/cm^2.

Figure 3 shows the major geological structures across the Pinglin Tunnel. Named in a west to east sequence, they include the following: the Yingtzulai Syncline, the Shihtsao Fault, the Taotiaotzu Syncline, the Shihpai Anticline, the Shihpai Fault, the Tachingmen Fault, the Paling Fault, the Shanghsin Fault, the Chinying Fault, and so on. The rock mass quality can roughly be divided into two major groups: That occurring between stations 27k + 750 ~ 36k is sound, and on average fair to good; between stations 36k ~ 40k + 681 the rock mass is inferior, averaging poor in grade. The possible cause of this is that strong shearing was prevailing during folding and faulting in the Penglai Orogency, which was followed by a series of normal faulting resulting from the extensional spreading of the Okinawa trough, rendering the rock mass severely fractured.

The Need for a Tunnel Boring Machine (TBM)

Except sections of several hundred meters from the portals, which are being constructed by Drill & Blast (D&B) Method, the major portion of the three tunnels will be excavated by three telescopic TBMs. The main considerations in adopting TBMs are:

1) Topography and Environment Considerations

The west portal of the Pinglin Tunnel is located on the left bank of the Peishih creek which is immediately upstream of the Feitsui reservoir, the main source of water supply for metropolitan Taipei. Not only the acquisition of land is extremely difficult but the massive haulage and disposal of excavated materials in the watershed of the reservoir during construction is also legally not allowed.

During the design stage, studies were made to find suitable sites for access adit(s) for increasing work faces to shorten the construction period. But, unfortunately, the conclusion was that the shortest adit would be 2.4 km in length with a continuous slope of -8%, which was impracticable and unsafe. Therefore, the only way is to advance the tunnel from the east portal towards the west portal. Further analysis reveals that if a D&B with an average advance rate of 60 meters per month was employed, it would take 18 years to hole through. On the contrary, if a TBM with an average advance rate of 300 meters per month was used, it would take only 3.5 years.

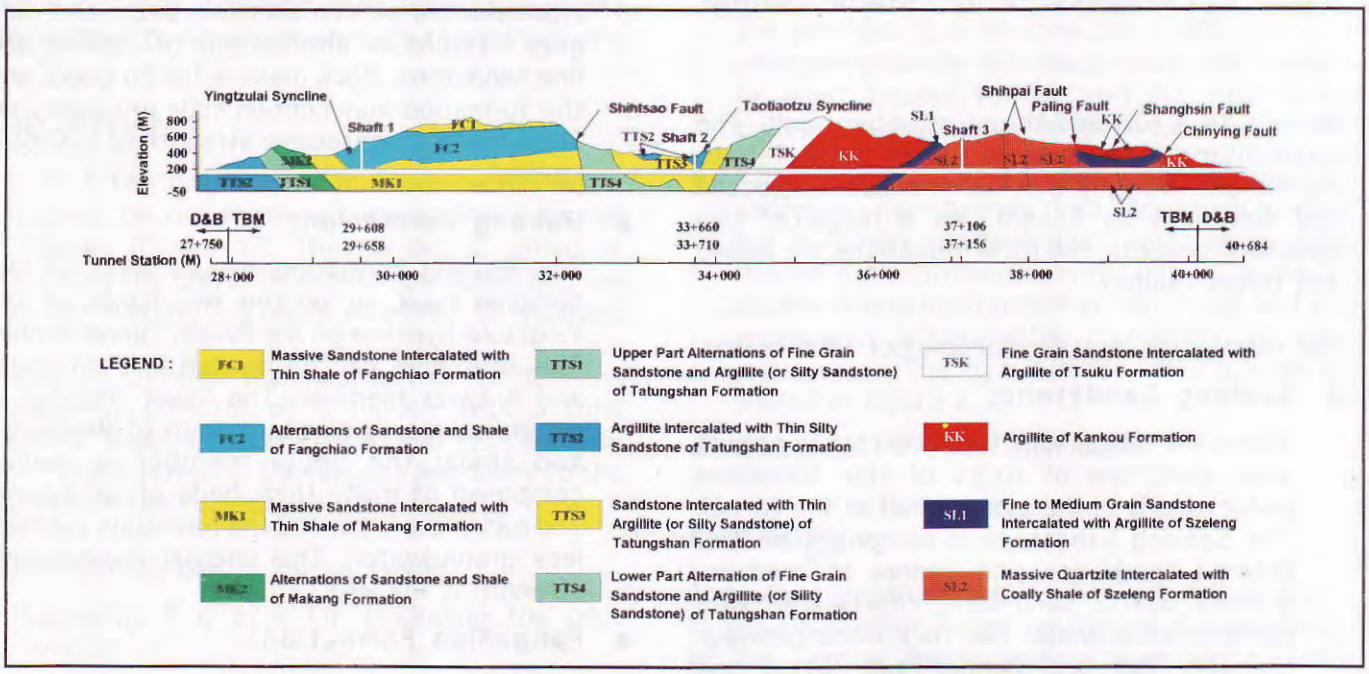

Figure 3: Geological Profile of Pinglin Tunnel

2) Geological Considerations

As shown in Figure 3, the geological profile of the Pinglin Tunnel is such that 3.5 km of the east portion is of argillite and Szeleng sandstone which are fractured in nature, and the remaining west portion of more than 9 km is mainly of sandstone, shale, and alternation of argillite and sandstone with strengths ranging from 400 to 1200 kg/cm^2. In other words, three-fourths of the ground condition is suitable for TBM tunnelling.

3) Labor Market and Economic Considerations

Assuming no other restrictions and according to international records and experiences, the advance rate of TBM is about 5 times that of the conventional D&B method. In other words, at least 5 work faces are needed by the D&B method to complete the tunnel for the same schedule requirement. Furthermore, on the assumption that each work face needs the same amount of labor, the labor force required for D&B tunnelling is about 5 times that needed for TBM. With recent labor market and wage levels in Taiwan taken into consideration, if D&B tunnelling was employed for the Pinglin Tunnel, there would be serious problems of labor shortage and higher cost as compared with the TBM method.

In order to cope with the fractured grounds and for safety reasons, a double shield hard rock TBM was selected for the pilot tunnel. Figure 4 shows the appearance of the 4.8 m diameter pilot TBM. Table 1 presents its technical data.

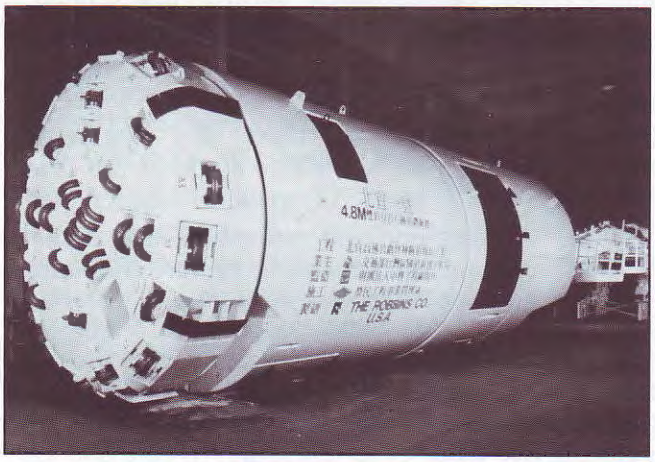

Figure 4: TBM for the Pinglin Pilot Tunnel

Table: 1: Technical Data of Pinglin Pilot Tunnel TBM

A. TBM			
1.	Type/Model	:	Robbins/153-269, Double Shields, Mixed Support
2.	Cutterhead Diameter/ Length of TBM	:	4.819 m ~ 4.8 m/ 10.833 m
3.	Forward Shield Outer Diameter (Include Stabilizer Shoe)	:	4.758 mm
4.	Tail Shield Taper/Outer Diameter: of Shield at Rear Edge		38 mm/4720 mm
5.	Number of Cutterhead Motors/ Motor Shaft Output Power	:	6/160 kW (Electrical Water Cooling)
6.	Cutterhead Speed, Low Speed/ High Speed	:	4.0 ~ 4.9 rpm/ 8 ~ 9.8 rpm (Before Modification)
7.	Cutterhead Torque, Low Speed/ High Speed	:	2030 kNm/1015 kNm
8.	Number of Primary Thrust Cylinders/Thrust Force	:	12/630 kN (Hydraulic Blacing)
9.	Number of Cutters/Size	:	34/432 mm (17 in)
10.	Main Bearing Diameter/Weight	:	3048 mm/3452 kg
11.	Number of Stabilizer Cylinders/ Thrust Force	:	2/2114 kN
12.	Number of Gripper/Cylinders/ Thrust Force	:	2/1572 kN
13.	Number of Auxiliary Thrust Cylinder/Thrust Force	:	8/2114 kN (Hydraulic Parallel)
14.	Segment Width/Thickness/ Outer Diameter	:	1.2 m/18 cm/4610 mm
15.	Minimum Excavating Radius	:	350 m
16.	Total Weight/total Capacity	:	360 t/1122 kW
B. Back-up System			
1.	Type/Number/Diameter/ Depth of Driller	:	Rotary & Percussion/ 2/76 mm/80 m
2.	Equipment for Gravel Backfill/ Grouting	:	Aliva 285/KG-15
3.	Wet Shotcrete Equipment/ Working Rate	:	Aliva 285/4 m^3/hr
4.	Number of Conveyors/Capacity	:	3/6 m^3/min
5.	Muck Car Power/Capacity/ Speed	:	Hydraulic/10*8 m^3/ 15 km/hr
6.	Total Length/Total Weight/ Capacity	:	177 m/360 t/500 kW

Difficult Conditions Encountered

The previous geologic investigations indicate that in the approximately 3.5 km long eastern portion of the Pinglin Tunnel there are five faults and intensively sheared or fractured zones. Particularly in the area between the east portal and the Chinying Fault, highly weathered and fractured argillite with plenty of groundwater prevails, which makes it very difficult for hard rock TBM boring.

The pilot TBM commenced boring in December 1992. However, up to July 1994 the advance was only 343 meters due to the time and effort spent on fighting the difficult ground conditions. The difficult ground conditions encountered can be categorized as follows:

(a) Mud and fine rock debris which flowed into the front chamber and overloading the mucking system and finally stopped the TBM.

(b) Instability of face which created great pressures on the cutter hear and jammed its rotation.

(c) Rock block fall which intruded into the mucking bucket and jammed it.

(d) Fallen rock pieces which jammed the movement of the rear shield.

(e) After long lasting stoppage the inward convergency of surrounding weak zone stuck the machine.

During the one and a half years operation of the pilot TBM, seven stoppages were experienced. The aforesaid scenario (b) was the most frequent occurrence. Two stoppages took place due to combination of scenarios (a) and (b); scenario (c) was usually found in conjunction with scenario (a) and/or scenario (b); scenarios (d) and (e) occurred respectively in February and May 1994 at the end of escape from scenario (b) stoppage.

In order to probe the ground conditions ahead of the TBM, advance drilling from the rear shield through built-in guide tubes has been specified in the contract. The probe holes shall be 30 m in length and least 10 m overlapped with the previous drilling. Consolidation grouting or other pretreatment measures are required when the probe reveals poor ground conditions. However, probe drilling and grouting was not efficient. The main reasons are:

- The built-in guide tubes are too small (ID = 80 mm) to use a more powerful drill and the space in the machine is limited for the drilling operation.
- The effective length of the 30 m long drilling hole is only 10 m long.
- Probing holes collapse easily due to intensively sheared and fractured ground.
- Identification of rock conditions ahead of the TBM is difficult unless a completed core has been taken. But to do that would take a much longer time.
- Consolidation grouting is difficult in clay seams prevailing in the fractured argillite, resulting in little ground improvement.

The difficulties in probing and grouting further slowed down the performance of the TBM.

Methods Used for Boring Through the Difficult Ground

The following steps were taken for driving through the difficult ground as represented by the various scenarios.

A. For scenario (a)

1. Drilling drainage holes from the guide tubes at the rear shield or from a working adit excavated on one side to release the groundwater pressure.
2. Cleaning up the intruded fine material to recover the functions of the belt conveyer and related equipment in the telescopic shield.
3. Carrying out chemical grouting (ARON-SR-US or Bentonite) to form a protection layer around the surface of the cutterhead and the telescopic shields to prevent possible bonding of cement grout.
4. Drilling holes and performing grouting from the guide tubes at the rear shield to consolidate the fractural rocks in front of the cutterhead. The extent of the consolidation grouting was about 30 m in length and twice the diameter of the tunnel in width and above the springline of the tunnel.
5. Withdrawing the cutterhead for a certain distance and trying to restart the machine and resuming the excavation.
6. If step 5 was not successful, excavation of a by-pass tunnel would be done as the last resort. All the collapsed material piled against the cutterhead was removed so that the machine could resume its normal operation.

The first and second stoppages of the pilot TBM occurred in January and May 1993 respectively.

The method of escape used was exactly the process described above. The first escape consumed 93 days and the second 52 days, both including some days for machine modifications. Modifications carried out during the first stoppage included welding grid bars on the muck bucket to prevent intrusion of over size rock blocks; adding wear strips on the surface of the cutterhead; installing a muck ring to prevent excessive muck from falling on the belt conveyer; installing a CCTV to monitor the mucking systems; enlarging the opening at the lower part of the tail shield to help the installation of precast segments; improving the guide beam of the probe drill and enlarging the diameter of the guide tubes from 80 mm to 94 mm so that a larger and more powerful casing drill could be used for the probing and grouting drilling. Modifications made during the 52 days of the second stoppage included the closure of three of the six buckets to reduce the muck inflow; welding of inclined plates on the corners of the cutterhead to reduce friction force; and continued enlargement of the guide tubes (16 holes in total).

B. For scenarios b and/or c

Because no water was encountered in these scenarios, step 1 was neglected. If no consolidation grouting was required prior to driving the by-pass tunnel (due to ungroutable ground, for instance), steps No. 3 and 4 were omitted too. The third through seventh stoppages of the pilot TBM were all of this type. In this case, the cutterhead was jammed by great amounts of collapsed material and became unmovable. The aforesaid step 5 was the first try. Step 6 was applied when step 5 failed.

Figure 5 shows the layout of a typical by-pass tunnel. Normally, the length of the by-pass tunnel from the tail shield to front face of the cutterhead is approximately 30m. The time required to excavate a by-pass tunnel including freeing of the cutterhead was about 30 days. As a matter of fact, the time spent for the third, fourth and the fifth stoppages were 37 days, 61 days and 45 days respectively. By use of the by-pass tunnel, some activities besides freeing the cutterhead were carried out. The activities included 1) excavating by means of drill and blast the top heading to remove the fractural zones in front of the TBM and support the rock with steel ribs, shotcrete and rock bolts; 2) using the by-pass tunnel as a working adit to drill holes for probing and drainage; 3) during the fourth stoppage, adding a reversible device to the cutterhead to help the machine escape from being jammed; 4) during the fifth stoppage, installing a 120° shroud plate at the front edge of the front shield above the cutterhead

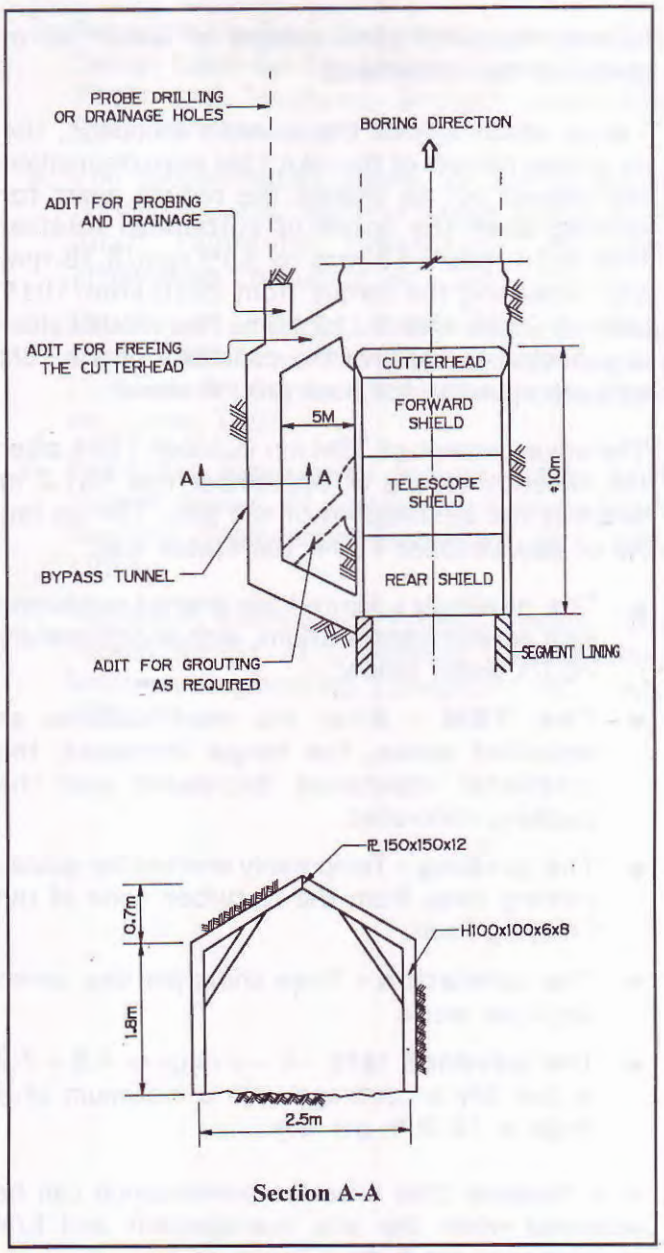

*Figure 5: **Typical Layout of Bypass Tunnel***

to protect the cutterhead from being directly hit and/or buried by collapsed rocks.

When driving through the Chinying Fault, the sixth stoppage occurred in May and the seventh in July 1994. In the sixth stoppage, there was no water intrusion, but a layer of about 12 m in width of squeezing gauge was encountered. The seventh stoppage was caused by the collapse of intensively sheared zones of broken sandstone with some water inflow. For these two stoppages, beside the by-pass tunnels, top headings of 20 m and 16 m in length were excavated and probing/drainage holes 39m and 77m long respectively were drilled. A steady discharge of more than 20 l/s from the 77 m probing hole revealed that a groundwater

bearing fractured zone existed at about 30 m ahead of the cutterhead.

Taking advantage of the seventh stoppage, the six driving motors of the pilot TBM were dismantled and moved out to change the reduce gears for slowing down the speed of cutterhead rotation from 4.56 rpm/9.12 rpm to 3.19 rpm/6.38 rpm and increasing the torque from 2030 kNm/1015 kNm to 2639 kNm/1319 kNm. This modification is expected to improve the capability of the TBM to overcome the fractural ground ahead.

The advancement of TBM ion October 1994 after the seventh escape of September was 181.2 m which is the best record of the pilot TBM so far. As of late October 1994, the status was:

- **The geology** - Jointed fine grained sandstone with argillite intercalations, with approximately 70 l/s water inflow.
- **The TBM** - After the modifications as described above, the torque increased, the rotational resistance decreased and the mucking controlled.
- **The probing** - Temporarily omitted for quickly running away from the disturbed zone of the Chinying Fault.
- **The operation** - Three shifts per day, seven days per week.
- **The advance rate** - 4 ~ 6 rings or 4.8 ~ 7.2 m per day on average with a maximum of 9 rings or 10.8 m per day.

It is foreseen that a better performance can be achieved when the site management and E/M maintenance are further improved.

Lessons Learned

The lessons learned from the driving of the Pinglin pilot tunnel by TBM are as follows:

- For a long tunnel project with unfavorable topographical conditions, strict environmental requirements, limited construction period and shortage of labor, to drive tunnels using TBMs is the sole feasible selection as long as geology is favorable.
- To deal with complicated ground conditions with faults or intensively fractured zones, plenty of groundwater and hard/soft mixed rock formations, the proper design of the TBM is extremely important. In other words, the TBM should not only have high torque, high thrust and penetration force, but also its cutterhead should be as short and smooth as possible, with appropriate tapered shields, and the much openings should be variable and controllable.
- Because of lack of TBM experience in the beginning, and for technology transfer and progress considerations, all members of the crew including foremen, TBM operators, E/M maintenance technicians and essential technical labor should come from an experienced foreign company. The local members would work as assistants or trainees. Operation by local members should take place gradually only when the TBM performance and progress are smooth and steady.
- Because of the geological variety and complexity in Taiwan, a longer learning period may be necessary for a TBM tunnelling project. A reasonable additional time allowance should be considered in the contract schedule.
- In the Pinglin pilot tunnel experience, the time for freeing a stuck TBM (double shields) was around forty to ninety days. Actually, these time periods included some days for mechanical modifications and/or ground treatments in front of the TBM. However, if no modification or treatment was required, the time for the escape of the TBM could be within thirty days.
- For such fractured ground conditions, the probe drilling took too much time due to repeated hole collapse (for a 30 m probe hole, as specified in the contract, the drilling should be completed in 2 hours, but actually it never took less than 6 hours). And if the probe showed the ground in need of consolidation grouting, at least some five more days would be required. Unfortunately, the effectiveness of consolidation grouting proved to be very limited due to the presence of clay in the rock seams. On the other hand, the frequent long stoppages (for drilling) may induce face collapse which could jam up the cutterhead. Therefore, it seems that probe drilling may be specified as an option.
- Based on the previous geological investigation, the design consultants did suggest that the first kilometer from the east portal should preferably be excavated by the drill and blast method. But unfortunately, the contractor commenced TBM boring at 520 m from the east portal and suffered very poor ground conditions until passing the Chinying Fault at about 900 m from the portal. The rock after Chinying Fault as a matter of fact, has proved to be much better recently. This reveals that geological investigations are very important and the construction method should be selected according to the findings.

The TBM is being used for the first time in Taiwan on the Pinglin Pilot Tunnel. Although the experience has been hard and painful, many useful lessons have been learned which doubtlessly will be helpful to the local tunneling industry in the future. It is foreseen that more and longer tunnels will be constructed in the next decade. These long tunnels will penetrate the complex geology in the Central Mountain region, which is similar to that of the Pinglin Tunnel. And the experience on the Pinglin Pilot Tunnel will provide a guide for the successful application of TBMs to these future long tunnel projects.

References

1. Nanking-Ilan Expressway Route Selection Study Geological Investigation for the Pinglin Tunnel (Final Report), Sinotech Engineering Consultant Inc., May 31, 1990.
2. Nankang-Ilan Expressway Project in Route Selection Final Report of Geological Investigation Work for Nankang Pinglin Section & Ilan Plain Section Contents, Moh and Associates, Inc., May, 1990.
3. Report on the Geological Investigation for Basic Design Taipei-Ilan Expressway Section Between Pinglin and Toucheng, Sinotech Engineering Consultant Inc., Mar., 1991.
4. The Supplementary Boring for the Geological Survey of Detail Design of Pinglin Tunnel No. 3 Shaft Taipei-Ilan Expressway, Sinotech Engineering Consultant Inc., Sept., 1992.
5. Final Report on Geological Exploration for Detail Design of Taipei-Ilan Expressway Project (Volume I-II), Sinotech Engineering Consultant Inc., June, 1993.
6. Taipei-Ilan Expressway Project Pinglin Pilot Tunnel Report of Geological Investigation, Sinotech Engineering Consultant Inc., July, 1992.
7. Taipei-Ilan Expressway Project Pinglin Pilot Tunnel Report of Geological Investigation, Sinotech Engineering Consultant Inc., July 1993.